Nanoscale

PAPER

Nearly lattice matched all wurtzite CdSe/ZnTe type II core–shell nanowires with epitaxial interfaces for photovoltaics†

Cite this: *Nanoscale*, 2014, **6**, 3679

Kai Wang,‡[a] Satish C. Rai,‡[a] Jason Marmon,[b] Jiajun Chen,[a] Kun Yao,[a] Sarah Wozny,[a] Baobao Cao,[a] Yanfa Yan,[c] Yong Zhang*[d] and Weilie Zhou*[a]

Achieving a high-quality interface is of great importance in core–shell nanowire solar cells, as it significantly inhibits interfacial recombination and thus improves the photovoltaic performance. Combining thermal evaporation of CdSe and pulsed laser deposition of ZnTe, we successfully synthesized nearly lattice matched all wurtzite CdSe/ZnTe core–shell nanowires on silicon substrates. Comprehensive morphological and structural characterizations revealed that a wurtzite ZnTe shell layer epitaxially grows over a wurtzite CdSe core nanowire with an abrupt interface. Further optical studies confirmed a high-quality interface and demonstrated efficient charge separation induced by the type-II band alignment. A representative photovoltaic device has been demonstrated and yielded an energy-conversion efficiency of 1.7% which can be further improved by surface passivation. The all-wurtzite core–shell nanowire with an epitaxial interface offers an attractive platform to explore the piezo-phototronic effect and promises an efficient hybrid nano-sized, energy harvesting system.

Received 19th November 2013
Accepted 10th January 2014

DOI: 10.1039/c3nr06137j

www.rsc.org/nanoscale

1. Introduction

Nanowire solar cells, which consist of either an individual nanowire or a nanowire array, have demonstrated great potential to power nanodevices and deliver high energy-conversion efficiency in an affordable manner.[1,2] Nanowires are beneficial for a number of reasons. In terms of light management, nanowires exhibit strong geometry-dependent absorption through a wave-guiding effect or optical interference when their diameter is smaller than or comparable to the excitation wavelength.[3–5] By imposing novel, device-physics concepts to manipulate light in nanowires, an impressive efficiency of 13.8% has been achieved in an InP nanowire array based solar cell.[6] In terms of carrier separation and collection, the single-crystalline nature and small diameter of nanowires enable efficient carrier transports along and across a nanowire's axis. The radial transport, also known as lateral charge separation, principally allows for greater tolerance of material defects. In practice, most nanowire solar cells exhibit inferior energy-conversion efficiency in comparison to their planar counterparts. This likely results from severe interfacial recombination originating from the materials' imperfection present along the interface between the core and shell, as well as the surface recombination.[7–10] Core/shell nanowires, however, are recognized as an optimal nano-architecture for light harvesting.[9,10] Recent progress on surface passivation of nanowires has shown noticeable enhancement in photovoltaic (PV) device performance.[11] Further performance improvements to core–shell nanowire solar cells require a high-quality interface between the core and the shell, in order to reduce the formation of interfacial structural defects that might act as trapping centers for the carriers. For instance, a good efficiency of 5.4% has been demonstrated in a single nanowire solar cell based on the CdS/Cu_2S core–shell nanowire, where a high-quality interface was created through a cation-exchange approach.[12]

One may expect a high-quality interface between the core and shell, if the shell can grow epitaxially over the core using the core as a growth template. In order to initialize a heteroepitaxial growth, several factors must be taken into account, such as lattice mismatch, difference in thermal expansion coefficient, and atomic inter-diffusion. CdSe and ZnTe stand out as an optimal combination in the II–VI semiconductor materials for constructing a high quality heteroepitaxial junction because of their small lattice mismatch, similar thermal expansion coefficients, type-II band offset and well-established doping capability.[13] Notably, the type-II CdSe/ZnTe core–shell structure has an effective bandgap around 1.1 eV, which is similar to Si and

[a]*Advanced Materials Research Institute, University of New Orleans, New Orleans, LA 70148, USA. E-mail: wzhou@uno.edu; Tel: +1 504-280-1068*

[b]*Nanoscale Science PhD Program, University of North Carolina at Charlotte, Charlotte, NC 28223, USA*

[c]*Department of Physics and Astronomy, University of Toledo, Toledo, OH 43606, USA*

[d]*Department of Electrical and Computer Engineering, University of North Carolina at Charlotte, Charlotte, NC 28223, USA. E-mail: yong.zhang@uncc.edu; Tel: +1 704-687-8652*

† Electronic supplementary information (ESI) available. See DOI: 10.1039/c3nr06137j

‡ These authors contributed equally to this work.

$CuInGaSe_2$, despite the fact that CdSe and ZnTe are wide bandgap semiconductors.[10]

Previous work with CdSe/ZnTe core–shell nanocrystals has demonstrated the promise of this material combination, such as an ultrafast hole transfer, an extended absorption profile and interfacial band emission.[14–16] However, efforts to synthesize a CdSe/ZnTe core–shell nanowire by a solution-phase approach resulted in a discontinuous shell layer or nanoislands of ZnTe on CdSe quantum wires.[17] Despite a few reports with special emphasis on the materials synthesis, to date, there have been no studies on CdSe/ZnTe or ZnTe/CdSe core–shell nanowire optoelectronics. This is primarily due to inferior interface and shell layer quality.[17]

In this work, we report the synthesis of CdSe/ZnTe core–shell nanowires using a two-step technique combining thermal evaporation and pulsed laser deposition (PLD) that has achieved epitaxial interfaces with a homogeneous wurtzite (WZ) ZnTe coating and abrupt interface, and a PV device processed from a single CdSe/ZnTe core–shell nanowire. The CdSe/ZnTe core–shell nanowire PV device demonstrated an energy-conversion efficiency of ~1.7%. The high-quality interfaces observed in the core–shell nanowire, along with their piezoelectric wurtzite phases render them ideal for achieving high-performance optoelectronics and harvesting multiple forms of energies.

2. Experimental

Synthesis of CdSe nanowires on a silicon substrate by thermal evaporation

The thermal evaporation of CdSe was conducted in a horizontal tube furnace under a mixed atmosphere of Ar/H_2 (4:1). Briefly, 0.1 g of CdSe powder (Alfa Aesar, 99.95% purity, metal basis) was loaded into an alumina crucible and positioned in the center of the furnace's quartz reactor. A silicon substrate was sputtered with 10 nm of gold and loaded into the downstream portion of the quartz reactor. The reactor was pumped down to 30 mTorr in order to eliminate residual oxygen and backfilled with inert gases (Ar/H_2), and then brought to atmospheric pressure with Ar/H_2 gases. The reactor temperature was ramped to 770 °C at a rate of 25 °C min^{-1}, and held there for 45 min under 150 sccm flow of Ar/H_2 gases. The silicon substrate was allowed to cool naturally to room temperature and the CdSe nanowires were collected on the silicon substrate.

ZnTe shell deposition by PLD

In order to synthesize CdSe/ZnTe core–shell nanowires, the silicon substrate with as-grown CdSe nanowires was transferred into a pulsed laser deposition system. ZnTe powder (99.95%, Alfa Aesar) was cold-pressed into a pellet and used as the deposition source. The distance between the target and silicon substrate was 40 mm. The system was pumped down to 30 mTorr and the temperature was increased to 350 °C before the laser beam was directed to the target. A Nd:YAG laser (LOTIS-TII, LS2147) was used to ablate the target. The laser-beam energy was set to 360 mJ cm^{-2} and had a wavelength of 1064 nm when the frequency was 5 Hz. The deposition was performed for 15 min, and the final product was collected for structural and optical characterizations and device fabrication.

Structural and optical characterizations

Structural and morphological characterizations were carried out with a Philips X'Pert-MPD X-ray diffractometer (XRD), a Carl Zeiss 1530 VP field-emission scanning electron microscope (SEM), and an FEI Tecnai F20-UT high-resolution transmission electron microscope (FETEM) equipped with a nanoprobe energy-dispersive X-ray spectroscope (EDS). Room temperature Raman spectroscopy and photoluminescence (PL) measurements were carried out using a Horiba LabRAM HR800 μ-Raman system. The data were collected with a 100× MPLAN objective lens (N.A. ≈ 0.9) in the backscatter configuration using a Horiba Synapse charge-coupled detector (CCD), and a Torus CW 532 nm laser.

PV device fabrication and electrical measurement

To fabricate photovoltaic devices, the CdSe/ZnTe core–shell nanowires were first removed from the collecting substrates and then dispersed in alcohol. The nanowire suspension was then dropped on the silicon substrate, which had a thermal oxide layer. The electrodes were fabricated by photolithography. Electron beam lithography was carried out three times during the whole process to achieve the final devices. The devices were ready for testing the photovoltaic properties after being stabilized in air for at least 12 hours. A standard solar simulator (Newport, Oriel) with calibrated 1-sun intensity was used in conjunction with a semiconductor characterization system (Keithley, 4200SCS) to obtain all device transport characteristics.

3. Results and discussion

Fig. 1(a) and (b) show representative SEM images of CdSe nanowires collected on silicon substrates. The nanowires were straight and several micrometers in length. The nanowires were randomly orientated on the substrate, and were well separated with a low density. As shown in the cross-sectional SEM images (Fig. 1(b)), the nanowires were grown directly on the micrometer-size CdSe grains, which had a thickness of ~2 μm. Fig. 1(c) and (d) represent the top- and cross-sectional views of a CdSe nanowire coated with ZnTe. A few small ZnTe particles, with a flower-bud-like morphology, covered the gold catalyst on the nanowire tips. ZnTe nanoparticles were also observed on nanowire surfaces, and are attributed to the emission of microscopic particulates from ZnTe solid targets when irradiated by a laser beam.[18]

More structural and compositional characterization was performed on both CdSe nanowires and CdSe/ZnTe nanowires by TEM equipped with a nanoprobe EDS. Fig. 2(a) displays a low-magnification TEM image of a CdSe nanowire and the corresponding selected area electron diffraction (SAED) pattern. The nanowire exhibited a diameter around 80 nm. The gold catalyst was observed on the tip, suggesting the vapor–liquid–solid (VLS) growth mode.[19] The interplanar spacing, as measured with high resolution transmission electron microscopy (HRTEM), was

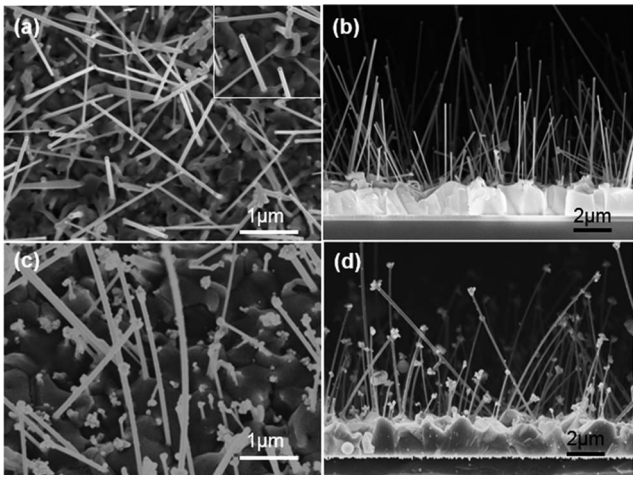

Fig. 1 CdSe and CdSe/ZnTe core–shell nanowire morphologies observed in SEM. CdSe nanowires grown on a silicon substrate by thermal evaporation observed from (a) top- and (b) cross-sectional views. CdSe/ZnTe nanowires imaged from the (c) top- and (d) cross-sectional views. Note the increased diameter from the shell and the nanoparticles on the tip and shell surface.

found to be 0.69 nm, as shown in Fig. 2(b). This, in combination with the sharp diffraction spots in Fig. 2(a), reveals that the CdSe nanowire is single crystalline in the wurtzite (WZ) structure with a preferential growth direction along the [0001] axis. Unlike ZnTe nanowires, which have an amorphous surface layer (see ESI Fig. S2†), the CdSe nanowires present smooth surfaces that favor epitaxial growth. A low magnification TEM image of a CdSe/ZnTe core–shell nanowire, shown in Fig. 2(c), confirms that occasional ZnTe nanoparticles are attached to the surface of the shell. Otherwise, CdSe/ZnTe core–shell nanowires exhibit a rather smooth external surface, which contrasts the highly mismatched ZnO/ZnSe and ZnO/ZnS core–shell nanowires reported previously by us.[20,21] Notably, no phase contrast was observed despite a rather thick shell, which is unusual in coaxial nanoscale heterostructures, and may result from the core and shell having nearly identical crystalline structures.[11,22,23] This assumption was confirmed by a convergent beam electron diffraction (CBED) pattern (Fig. 2(c), inset) of the core–shell nanowire – only one pattern was obtained. The CBED of a core–shell nanowire, which was identical to the SAED pattern of CdSe, was indexed as hexagonal WZ when the incident electron beam was along the $[2\bar{1}\bar{1}0]$ direction. The deposited ZnTe shell crystallizes into the same WZ structure as the WZ CdSe nanowire core. The core–shell interface, as examined by high-resolution imaging and presented as a dashed, yellow line in Fig. 2(d), can only be distinguished with the assistance of slightly distorted lattice fringes due to a small lattice mismatch of ~0.08% between WZ CdSe and WZ ZnTe. The core literally acts as a structural template for the shell. The shell thickness was measured to be 20 nm and it is tunable by adjusting the deposition time, laser power density and the distance between the

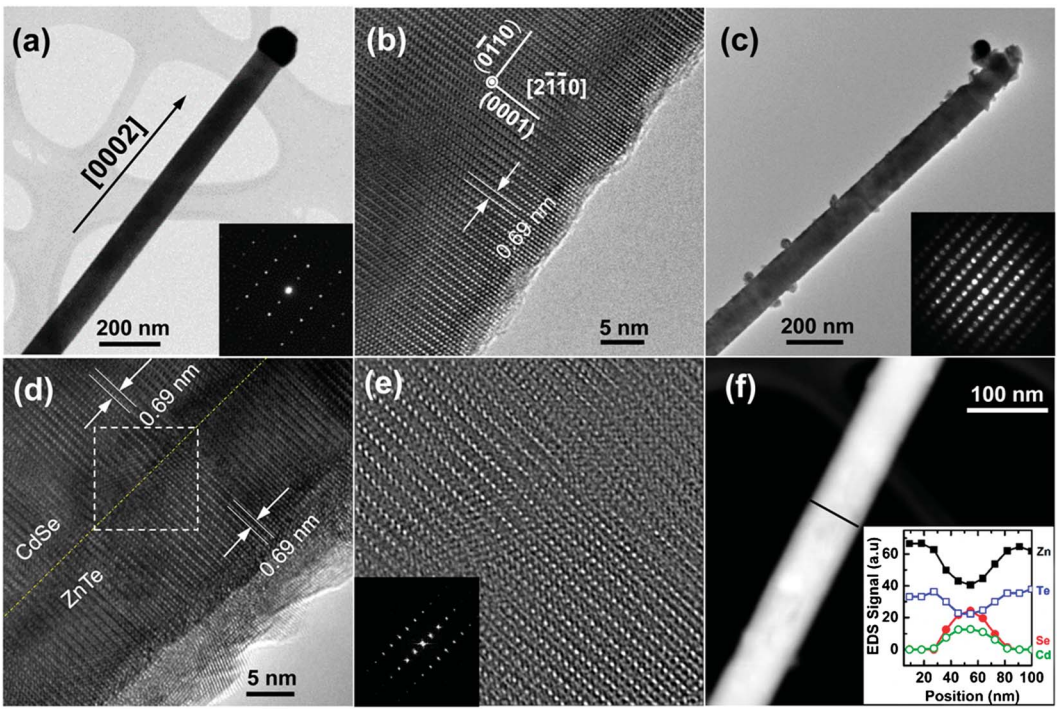

Fig. 2 Structural characterization of a CdSe nanowire and CdS/ZnTe core–shell nanowire. (a) Low magnification TEM image of an individual CdSe nanowire. Inset: the corresponding SAED pattern. (b) HRTEM of a CdSe nanowire demonstrating a single-crystalline, WZ structure. (c) A representative TEM image of an individual CdSe/ZnTe core–shell nanowire. Inset: the corresponding CBED pattern. (d) HRTEM images of the core–shell interface that display the interplanar spacing and epitaxial growth of the WZ ZnTe shell on the WZ CdSe core. (e) Inverse FFT image. Inset: core–shell interface processed from the white, dashed rectangle in (d). (f) A STEM image of a CdSe/ZnTe core–shell nanowire. Inset: EDS data obtained with a nanoprobe scan along the black line that extends axially across the interface.

target and CdSe nanowire template. An epitaxial growth relationship between the core and shell was determined to be $(0001)_{CdSe}//(0001)_{ZnTe}$ and $(0\bar{1}10)_{CdSe}//(0\bar{1}10)_{ZnTe}$ respectively using fast Fourier transform (FFT) of the interface area – refer to the area enclosed by a white rectangle in the inset of Fig. 2(e). The two-step technique used to fabricate the core–shell nanowires at elevated temperatures made interfacial diffusion between the core and shell a concern.[24–26] However, the FFT image in Fig. 2(e) highlights the high quality of the well-matched and continuous core and shell lattice fringes along the nanowire interface. Also, a nanoprobe EDS line scanning was employed to detect the compositional distribution across the radial junction of the core–shell nanowire. Fig. 2(f) shows a representative bright-field TEM image of a core–shell nanowire in the scanning transmission electron microscopy (STEM) mode, where the scan position is labeled with a black line. Within the spatial resolution and detection limit of the nanoprobe EDS, the elemental distribution data (Fig. 2(f), inset) imply no obvious diffusion of CdSe into the ZnTe shell. FFT and EDS line scan results are consistent in proving the growth of a high-quality and abrupt core–shell interface. The line-scan also confirmed a highly uniform ZnTe coating over CdSe nanowires. In comparison, an attempt to fabricate a ZnTe/CdSe core–shell nanowire *via* the same technique produced a discontinuous and rough CdSe shell layer (ESI Fig. S3†). This asymmetry in the growth sequence is rather interesting, deserving further study in the future.

CdSe/ZnTe core–shell nanowires were analyzed optically using photoluminescence and Raman spectroscopy. Isolated single CdSe nanowires and CdSe/ZnTe core–shell nanowires were excited by a 532 nm continuous wave laser. The corresponding PL and Raman emissions were measured at 300 K, as shown in Fig. 3(a). The CdSe nanowire PL spectrum consists of a single emission band centered at 1.734 eV, which closely matched the free-exciton emission energy in bulk CdSe.[27] Interestingly, the CdSe emission efficiency of the core–shell nanowire was observed to be over an order of magnitude lower than that of a representative, bare CdSe nanowire. This could indicate efficient charge separation of photogenerated electron–hole pairs across the CdSe/ZnTe interface as illustrated in the inset of Fig. 3(a). As the ZnTe layer increases, the charge separation induced by the staggered, type-II band alignment of this heterostructure gives rise to a further decrease in or even quenched emission (see ESI Fig. S4†). Similar findings were also reported for ZnO/ZnSe and ZnO/ZnS nanowire arrays and a single axial CdTe–CdSe heteronanowire.[20,21,28–30] However, the sharper interface and fewer dislocations of a lattice-matched CdSe/ZnTe system would enable further enhancement of charge separation. Furthermore, we also observed a slight (6 meV) emission red shift for the core–shell nanowires. This red shift could be ascribed to the strain present in a radial nanowire heterostructure,[31] although the strain across the interface in our core–shell nanowires is considerably lower due to the similarity of core and shell lattice constants.

Fig. 3(b) presents the Raman spectra of a representative individual CdSe nanowire, and CdSe/ZnTe core–shell nanowire, along with a CdSe thin film and bulk ZnTe measurements as references. The first- and second-order longitudinal optical

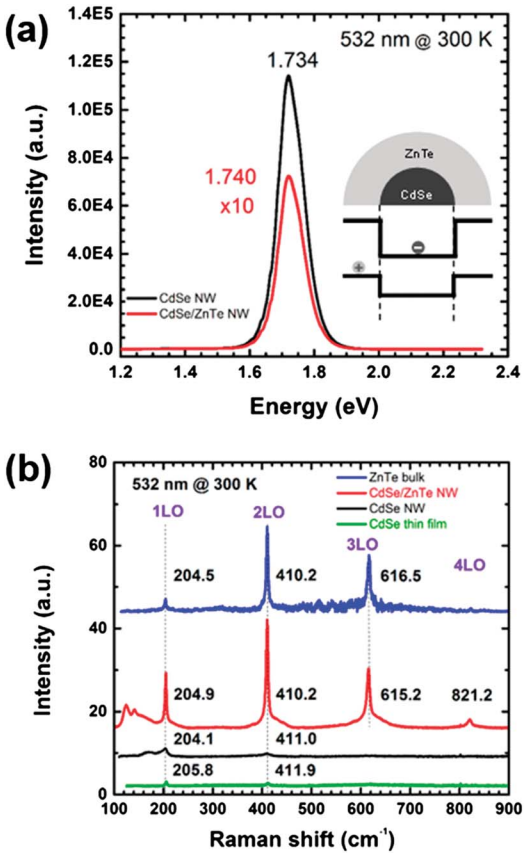

Fig. 3 Optical characterization of CdSe nanowires and CdSe/ZnTe core–shell nanowires. (a) Photoluminescence spectrum of a representative CdSe nanowire and CdSe/ZnTe core–shell nanowire. Inset: type-II heterojunction diagram of a CdSe/ZnTe core/shell structure. (b) Raman spectra of a representative CdSe nanowire and CdSe/ZnTe nanowires with spectra of bulk ZnTe and a CdSe thin film for reference.

(1- and 2-LO) phonon modes for a bare CdSe nanowire were identified at 204.1 cm^{-1} and 411.0 cm^{-1}. The 1-, 2-, 3-, and 4-LO phonon modes of the CdSe/ZnTe core–shell nanowire appeared at 204.9 cm^{-1}, 410.2 cm^{-1}, 615.2 cm^{-1}, and 812.2 cm^{-1} respectively, and are in very good agreement with the phonon modes measured in bulk ZnTe. Up to four orders of LO phonon modes were observed with 532 nm excitation in both bulk ZnTe and the CdSe/ZnTe core–shell nanowire.[32] This was possible due to the resonant condition where the excitation wavelength (2.33 eV) is above the bandgap of ZnTe (~2.3 eV), and also explains the absence of emission peaks from the ZnTe shell. Band gap emission from the shell, if any, is quenched due to charge separation induced by the type-II band alignment. The relatively high resonant-Raman intensity of the thin ZnTe shell further indicated ZnTe's crystalline quality, and also partially masked the CdSe signal. In addition, trigonal tellurium (Te) peaks, which were induced through a laser ablation, appeared at 124.3 cm^{-1} and 141.8 cm^{-1} and were assigned to the A1 and E_{TO} modes respectively.[33,34]

Bulk ZnTe is thermodynamically stable in a cubic zinc blende (ZB) structure, although it has been reported in the

hexagonal phase as nanocrystalline materials.[35–37] To the best of our knowledge, this is the first time the growth of single-crystalline WZ ZnTe on WZ CdSe was achieved. From a structural perspective, this intriguing observation opens avenues of exploration into more unique structures, such as WZ ZnTe nanotubes and 1D WZ CdSe–ZnTe superlattices or axial nanoheterostructures.[25,38–40] By deliberately controlling the growth conditions, the heterojunction's crystal structure and band gap can be engineered.[41] Also, when stress is applied, an additional piezoelectric potential is expected to be created in the WZ p-ZnTe layer on the WZ n-CdSe nanowire system, which will offer more freedom to manipulate the piezotronic effect.[42,43] In regards to the piezotronic effect, a vertically aligned CdSe nanowire array was proven as an ideal candidate for harvesting mechanical energy (also see ESI Fig. S5†).[44] More importantly, having both the core and shell crystallize in a wurtzite structure creates a heterojunction that is well matched to the solar spectrum; it also provides an ideal platform to probe the piezo-phototronic effect, as well as the harvesting of multiple forms of energy.[43,45]

Our PV device was fabricated from a single CdSe/ZnTe core–shell nanowire, as sketched in Fig. 4(a). The nanowire was placed on a SiO_2/Si substrate, with one end partially etched to expose the CdSe core, and two asymmetric electrodes deposited on each end. Indium and nickel were selected as the electrode materials for the CdSe core and ZnTe shell respectively.[46,47] Fig. 4(b) depicts a representative SEM image of this core–shell nanowire PV device. The current–voltage (I–V) characteristics under AM 1.5G illumination and the dark current were measured at 25 °C. As shown in Fig. 4(c), the device's dark I–V curve exhibits clear rectifying behavior. Under illumination, the rectifying curve shifts downwards due to the generation of photocurrent. The energy conversion efficiency, η, was evaluated using the geometric cross-section of the core–shell region as the active area of the device, because only the coaxial junction contributes to photocurrent generation.[12,48] It was calculated by dividing the maximum generated power, P_{out}, by the total incident power over the illuminated core–shell nanowire area, P_{in}. The best core–shell nanowire solar cell exhibited an open circuit voltage, V_{oc}, of 0.18 V, a short-circuit current, I_{sc}, of 38 pA, and a fill factor (FF) of 0.38, which yielded an η of 1.7%. Note that because the nanowire is relatively thin, the absorption is far from complete, the efficiency could be significantly underestimated. Although the obtained η was comparable to that in ZnTe/CdSe thin film solar cells, the V_{oc} was considerably lower than 1.1 V, which was the estimated effective bandgap energy of this type-II heterojunction, and suggested the existence of nonradiative recombination.[49] Because of the abrupt interface, as visualized with TEM, we associate nonradiative recombination mostly with surface states arising from the large surface-to-volume ratio in the nanostructured system, and the possible residue/defects induced by the wet-chemistry etching process. Future effort on surface passivation with a window layer, for example, ZnTe:Cu, to suppress the carrier recombination of these surface states is underway.[11]

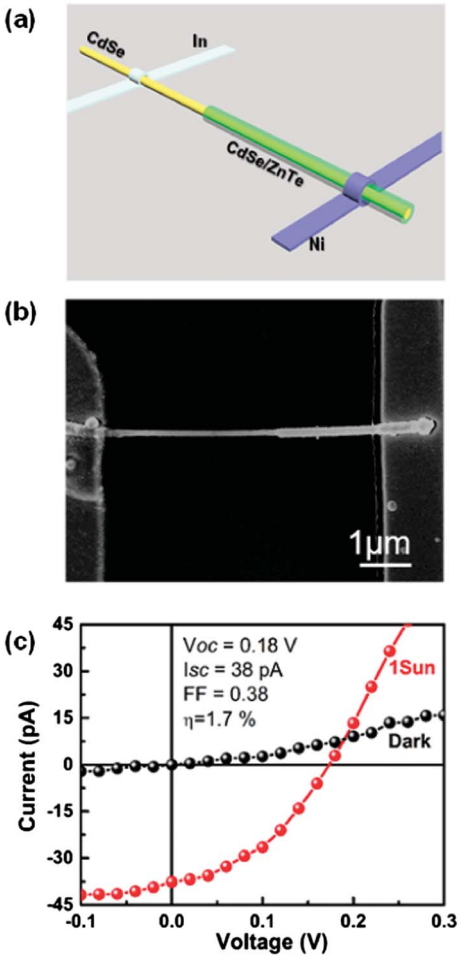

Fig. 4 Electrical characterization of a single core–shell nanowire PV device. (a) Schematics of a PV device based on an individual CdSe/ZnTe core–shell nanowire. The electrode materials for the core and shell are indium and nickel respectively. (b) A representative SEM image of a PV device. The ZnTe shell was partially etched by a saturated, aqueous $FeCl_3$ solution. (c) Current–voltage (I–V) characteristics for the best CdSe/ZnTe core–shell nanowire solar cell measured under AM 1.5G illumination and dark current. These are figures of merit for a PV device.

4. Conclusion

In conclusion, we have synthesized high-quality CdSe/ZnTe core–shell nanowires on a silicon substrate by combining the techniques of thermal evaporation and pulsed laser deposition. The CdSe/ZnTe core–shell nanowire exhibited a sharp, core–shell interface with a WZ structure throughout. An epitaxial relationship, $(0001)_{CdSe}//(0001)_{ZnTe}$ and $(0\bar{1}10)_{CdSe}//(0\bar{1}10)_{ZnTe}$, was determined for the CdSe/ZnTe core–shell structure. The photovoltaic device based on a single CdSe/ZnTe core–shell nanowire was fabricated, yielding an energy-conversion efficiency of ~1.7%. Considering the fact that the current device is apparently not optimized in many aspects, such as incomplete light absorption, lacking any surface passivation, there is much room to improve the efficiency by optimizing device configuration, material composition, and/or morphologies. For instance,

a vertically aligned array structure of the core/shell nanowires can significantly boost light collection, as explored in various other types of core/shell nanowire devices. The intriguing growth relationship observed in the coaxial heterostructure offers the opportunity to manipulate the shell's crystalline structure by controlling that of the core, regardless of the equilibrium crystal structure of the shell material. These findings also provide the possibility to understand the coupling effects of photovoltaic and piezoelectric devices in low dimensionality and how to harvest hybrid energy with either a single core–shell nanowire or a core–shell nanowire array.

Acknowledgements

We gratefully acknowledge financial support from the American Chemical Society Petroleum Research Fund PRF no. 48796-DNI10 and Louisiana Board of Regents Contract no. LA LEQSF(2011-13)-RD-B-08. Work at UNCC (J. M. and Y. Z.) was partially supported by the Bissell Distinguished Professorship endowment fund. K.W. also appreciates AFM and partial photoluminescence measurements performed by Susanne Schäfer at the University of Hamburg.

References

1 B. Tian, T. J. Kempa and C. M. Lieber, *Chem. Soc. Rev.*, 2009, **38**, 16–24.
2 M. Law, L. E. Greene, J. C. Johnson, R. Saykally and P. D. Yang, *Nat. Mater.*, 2005, **4**, 455–459.
3 L. Y. Cao, J. S. White, J. S. Park, J. A. Schuller, B. M. Clemens and M. L. Brongersma, *Nat. Mater.*, 2009, **8**, 643–647.
4 P. M. Wu, N. Anttu, H. Q. Xu, L. Samuelson and M.-E. Pistol, *Nano Lett.*, 2012, **12**, 1990–1995.
5 M. D. Kelzenberg, S. W. Boettcher, J. A. Petykiewicz, D. B. Turner-Evans, M. C. Putnam, E. L. Warren, J. M. Spurgeon, R. M. Briggs, N. S. Lewis and H. A. Atwater, *Nat. Mater.*, 2010, **9**, 239–244.
6 J. Wallentin, N. Anttu, D. Asoli, M. Huffman, I. Aberg, M. H. Magnusson, G. Siefer, P. Fuss-Kailuweit, F. Dimroth, B. Witzigmann, H. Q. Xu, L. Samuelson, K. Deppert and M. T. Borgstrom, *Science*, 2013, **339**, 1057–1060.
7 E. C. Garnett and P. Yang, *J. Am. Chem. Soc.*, 2008, **130**, 9224–9225.
8 M. M. Adachi, M. P. Anantram and K. S. Karim, *Sci. Rep.*, 2013, **3**, 1546.
9 B. M. Kayes, H. A. Atwater and N. S. Lewis, *J. Appl. Phys.*, 2005, **97**, 114302.
10 Y. Zhang, L.-W. Wang and A. Mascarenhas, *Nano Lett.*, 2007, **7**, 1264–1269.
11 J. V. Holm, H. I. Jørgensen, P. Krogstrup, J. Nygård, H. Liu and M. Aagesen, *Nat. Commun.*, 2013, **4**, 1498.
12 J. Y. Tang, Z. Y. Huo, S. Brittman, H. W. Gao and P. D. Yang, *Nat. Nanotechnol.*, 2011, **6**, 568–572.
13 M. C. Phillips, E. T. Yu, Y. Rajakarunanayake, J. O. McCaldin, D. A. Collins and T. C. McGill, *J. Cryst. Growth*, 1991, **111**, 820–822.
14 C.-H. Wang, C.-W. Chen, C.-M. Wei, Y.-F. Chen, C.-W. Lai, M.-L. Ho and P.-T. Chou, *J. Phys. Chem. C*, 2009, **113**, 15548–15552.
15 S. Kaniyankandy, S. Rawalekar, S. Verma and H. N. Ghosh, *J. Phys. Chem. C*, 2011, **115**, 1428–1435.
16 C. Y. Chen, C. T. Cheng, J. K. Yu, S. C. Pu, Y. M. Cheng, P. T. Chou, Y. H. Chou and H. T. Chiu, *J. Phys. Chem. B*, 2004, **108**, 10687–10691.
17 J. A. Goebl, R. W. Black, J. Puthussery, J. Giblin, T. H. Kosel and M. Kuno, *J. Am. Chem. Soc.*, 2008, **130**, 14822–14833.
18 L. Cultreraa, M. I. Zeifmanb and A. Perrone, *Appl. Surf. Sci.*, 2007, **253**, 6322–6325.
19 R. S. Wagner and W. C. Ellis, *Appl. Phys. Lett.*, 1964, **4**, 89–90.
20 K. Wang, J. Chen, W. Zhou, Y. Zhang, Y. Yan, J. Pern and A. Mascarenhas, *Adv. Mater.*, 2008, **20**, 3248–3253.
21 K. Wang, J. J. Chen, Z. M. Zeng, J. Tarr, W. L. Zhou, Y. Zhang, Y. F. Yan, C. S. Jiang, J. Pern and A. Mascarenhas, *Appl. Phys. Lett.*, 2010, **96**, 123105.
22 S. G. Ghalamestani, M. Heurlin, L.-E. Wernersson, S. Lehmann and K. A. Dick, *Nanotechnology*, 2012, **23**, 285601.
23 Y. L. Chueh, C. H. Hsieh, M. T. Chang, L. J. Chou, C. S. Lao, J. H. Song, J. Y. Gan and Z. L. Wang, *Adv. Mater.*, 2007, **19**, 143–149.
24 H. Jin fan, M. Knez, R. Scholz, K. Nielsch, E. Pippel, D. Hesse, M. Zacharias and U. Gosele, *Nat. Mater.*, 2006, **5**, 627–631.
25 K. Nagashima, T. Yanagida, H. Tanaka, S. Seki, A. Saeki, S. Tagawa and T. Kawai, *J. Am. Chem. Soc.*, 2008, **130**, 5378–5382.
26 W. I. Park, H. S. Kim, S. Y. Jang, J. Park, S. Y. Bae, M. Jung, H. Lee and J. Kim, *J. Mater. Chem.*, 2008, **18**, 875–880.
27 R. Chen, M. I. Bakti Utama, Z. Peng, B. Peng, Q. Xiong and H. Sun, *Adv. Mater.*, 2011, **23**, 1404–1408.
28 S. Schafer, A. Reich, Z. Wang, T. Kipp and A. Mews, *Appl. Phys. Lett.*, 2012, **100**, 022110.
29 Z. Wu, Y. Zhang, J. Zheng, X. Lin, X. Chen, B. Huang, H. Wang, K. Huang, S. Li and J. Kang, *J. Mater. Chem.*, 2011, **21**, 6020–6026.
30 Y. Zhang, Z. Wu, J. Zheng, X. Lin, H. Zhan, S. Li, J. Kang, J. Bleuse and H. Mariette, *Sol. Energy Mater. Sol. Cells*, 2012, **102**, 15–18.
31 O. D. D. Couto, D. Sercombe, J. Puebla, L. Otubo, I. J. Luxmoore, M. Sich, T. J. Elliott, E. A. Chekhovich, L. R. Wilson, M. S. Skolnick, H. Y. Liu and A. I. Tartakovskii, *Nano Lett.*, 2012, **12**, 5269–5274.
32 Q. Zhang, J. Zhang, M. I. B. Utama, B. Peng, M. de la Mata, J. Arbiol and Q. Xiong, *Phys. Rev. B: Condens. Matter Mater. Phys.*, 2012, **85**, 085418.
33 V. Wiedemeier, G. Berth, A. Zrenner, E. M. Larramendi, U. Woggon, K. Lischka and D. Schikora, *Semicond. Sci. Technol.*, 2011, **26**, 105023.
34 A. S. Pine and G. Dresselhaus, *Phys. Rev. B: Solid State*, 1971, **4**, 356–371.
35 E. Janik, J. Sadowski, P. Dluzewski, S. Kret, L. T. Baczewski, A. Petroutchik, E. Lusakowska, J. Wrobel, W. Zaleszczyk, G. Karczewski, T. Wojtowicz and A. Presz, *Appl. Phys. Lett.*, 2006, **89**, 133114.

36 J. Zhang, S. Jin, H. C. Fry, S. Peng, E. Shevchenko, G. P. Wiederrecht and T. Rajh, *J. Am. Chem. Soc.*, 2011, **133**, 15324–15327.
37 X. Y. Huang, J. Li, Y. Zhang and A. Mascarenhas, *J. Am. Chem. Soc.*, 2003, **125**, 7049–7055.
38 Z. Liu, D. Zhang, S. Han, C. Li, B. Lei, W. Lu, J. Fang and C. Zhou, *J. Am. Chem. Soc.*, 2004, **127**, 6–7.
39 S. C. Andrews, M. A. Fardy, M. C. Moore, S. Aloni, M. Zhang, V. Radmilovic and P. Yang, *Chem. Sci.*, 2011, **2**, 706–714.
40 S. Boyer-Richard, C. Robert, L. Gerard, J.-P. Richters, R. Andre, J. Bleuse, H. Mariette, J. Even and J.-M. Jancu, *Nanoscale Res. Lett.*, 2012, **7**, 543.
41 M. r. Hocevar, G. Immink, M. Verheijen, N. Akopian, V. Zwiller, L. Kouwenhoven and E. Bakkers, *Nat. Commun.*, 2012, **3**, 1266.
42 Z. L. Wang and J. Song, *Science*, 2006, **312**, 242–246.
43 Y.-F. Lin, J. Song, Y. Ding, S.-Y. Lu and Z. L. Wang, *Adv. Mater.*, 2008, **20**, 3127–3130.
44 Y. S. Zhou, K. Wang, W. Han, S. C. Rai, Y. Zhang, Y. Ding, C. Pan, F. Zhang, W. Zhou and Z. L. Wang, *ACS Nano*, 2012, **6**, 6478–6482.
45 C. Pan, S. Niu, Y. Ding, L. Dong, R. Yu, Y. Liu, G. Zhu and Z. L. Wang, *Nano Lett.*, 2012, **12**, 3302–3307.
46 Z. He, J. Jie, W. Zhang, W. Zhang, L. Luo, X. Fan, G. Yuan, I. Bello and S.-T. Lee, *Small*, 2009, **5**, 345–350.
47 Q. F. Meng, C. B. Jiang and S. X. Mao, *Appl. Phys. Lett.*, 2009, **94**, 043111.
48 C. Colombo, M. Heibeta, M. Gratzel and A. F. i. Morral, *Appl. Phys. Lett.*, 2009, **94**, 173108.
49 N. G. Patel, C. J. Panchal, K. K. Makhija, P. G. Patel and S. S. Patel, *Cryst. Res. Technol.*, 1994, **29**, 247–252.